Available online at www.sciencedirect.com

ScienceDirect

Green Energy & Environment 5 (2020) 423–432

www.keaipublishing.com/gee

Research paper

Structured NiFe catalysts derived from in-situ grown layered double hydroxides on ceramic monolith for CO_2 methanation

Huong Lan Huynh [a], Wakshum Mekonnen Tucho [b], Zhixin Yu [a,*]

[a] Department of Energy and Petroleum Engineering, University of Stavanger, 4036 Stavanger, Norway
[b] Department of Mechanical and Structural Engineering and Material Science, University of Stavanger, 4036 Stavanger, Norway

Received 29 July 2020; revised 11 September 2020; accepted 17 September 2020
Available online 28 September 2020

Abstract

Monolithic catalysts for CO_2 methanation have become an active research area for the industrial development of Power-to-Gas technology. In this study, we developed a facile and reproducible synthesis strategy for the preparation of structured NiFe catalysts on washcoated cordierite monoliths for CO_2 methanation. The NiFe catalysts were derived from in-situ grown layered double hydroxides (LDHs) via urea hydrolysis. The influence of different washcoat materials, i.e., alumina and silica colloidal suspensions on the formation of LDHs layer was investigated, together with the impact of total metal concentration. NiFe LDHs were precipitated on the exterior surface of cordierite washcoated with alumina, while it was found to deposit further inside the channel wall of monolith washcoated with silica due to different intrinsic properties of the colloidal solutions. On the other hand, the thickness of in-situ grown LDHs layers and the catalyst loading could be increased by high metal concentration. The best monolithic catalyst (COR-AluCC-0.5M) was robust, having a thin and well-adhered catalytic layer on the cordierite substrate. As a result, high methane yield was obtained from CO_2 methanation at high flow rate on this structured NiFe catalysts. The monolithic catalysts appeared as promising structured catalysts for the development of industrial methanation reactor.

Keywords: CO_2 methanation; Structured catalysts; In-situ growth; Layered double hydroxides; Ceramic honeycomb monolith

1. Introduction

The ever-growing concern on carbon dioxide mitigation has drawn much attention to sustainable solutions in the past decades. Carbon capture, utilization, and storage (CCUS) plays a major role to tackle this global climate change challenge. Most interestingly, carbon-neutral industrial processes in which renewable energy sources are utilized to convert CO_2 into valuable fuels and chemicals with no carbon footprint emerge as promising approaches for CO_2 utilization [1]. One of many potential processes is Power-to-Gas (PtG) technology which can produce methane or synthetic natural gas (SNG), an important chemical energy carrier with high heating value [2]. In this process, hydrogen produced via water electrolysis by excessive renewable electricity and captured carbon dioxides are catalytically converted to methane via the Sabatier reaction Eq. (1), also called CO_2 methanation.

$$CO_2 + 4H_2 \leftrightarrow CH_4 + 2H_2O,\ \Delta H_{298\ K} = -165.0\ kJ\ mol^{-1} \quad (1)$$

Catalytic CO_2 methanation is an exothermic reaction which thermodynamically favored at low temperatures and elevated pressures. However, due to unfavorable kinetics, high conversion rates are difficult to be achieved at low-temperature region of 200–350 °C. On the other hand, the reaction mechanism is still under debate despite being discovered for more than a hundred years [3,4]. Metals in group VIII are well-known as active catalysts for the CO_2 methanation. Although noble metals (i.e., Ru, Rh) have excellent activity and stability, Ni-

* Corresponding author.
E-mail address: zhixin.yu@uis.no (Z. Yu).

https://doi.org/10.1016/j.gee.2020.09.004

based catalysts are widely used for CO_2 methanation due to the affordable price and good performance [5–8].

A large number of research studies have been devoted to improving the activity of Ni-based catalysts for CO_2 methanation, especially at low temperatures over powder/pellet catalysts in fixed-bed reactor [9]. Many efforts have been dedicated to studying different type of supports, from single (e.g., Al_2O_3, TiO_2, SiO_2) to composite (e.g., Al_2O_3-SiO_2, CeO_2-ZrO_2) or novel type (e.g., mesoporous materials, molecular sieves, nanotubes, graphene, zeolite, etc.), often with different additives, such as alkaline and rare earth metal oxides, transition and noble metals. For example, Fe has been recognized as an excellent promoter, significantly improving the activity of Ni-based catalysts for low-temperature CO_2 methanation [10–12]. Besides, it should be emphasized that the performances of Ni-based catalysts are strongly impacted by the preparation methods. It has been recognized that catalysts prepared by layer double hydroxides precursors (LDHs, general formula $[M^{2+}_{1-x}M^{3+}_{x}(OH)_2](A^{n-})_{x/n} \cdot mH_2O$, where M are metals, and A is anion) exhibited higher activity and selectivity than catalysts prepared by conventional methods due to better dispersion of metal active sites [8,13].

The development of laboratory research into industrial practice is essential for the commercialization of PtG technology. One of the most recent development trends of methanation unit is structured reactors equipped with monolithic catalysts [14]. Structured catalysts and reactors have been widely used for environmental applications, such as automotive catalysts, volatile organic compounds incinerators, etc. Honeycomb monoliths have become the common catalyst shape after their commercial success for automobile exhaust treatment [15]. Therefore, the use of structured catalysts for other heterogeneous catalytic reactions has been highly motivated. Monolithic catalysts offer many advantages over conventional pelletized catalysts, such as lower pressure drop associated with the high flow rates and small size of the reactor, which are typical concerns for gas-phase chemical processes. For CO_2 methanation, monolithic catalysts can handle large volumetric flow of CO_2 during industrial applications with more efficient heat and mass transfer.

In terms of preparation methods, there are two types of structured catalysts. Catalysts in which an active phase is deposited on inert monolithic support are classified as coated catalysts, whereas catalysts in which the whole structure is made from the active compounds are bulk catalysts. Most structured catalysts used for CO_2 methanation were coated catalysts [13]. Cordierite ($2Al_2O_3 \cdot 5SiO_2 \cdot 2MgO$) is the most widely used ceramic material for the production of commercial monoliths with different dimensions and cell densities. Cordierite has high thermal stability and low thermal expansion coefficient, but ultralow surface area. Therefore, it is advantageous to coat a layer of support material on cordierite in order to increase the surface area prior to the deposition of active catalyst layer. The active layer can be deposited by different methods such as impregnation or deposition–precipitation [16].

The main concern is the homogeneous distribution of the active phase on monolithic support. Recently, a novel synthesis using urea hydrolysis to deposit LDHs layer in-situ on structured supports as precursors for structured catalysts has been reported. In the presence of a basic retardant, i.e., urea, LDHs consisting of Ni-Al, Co-Al, Co-Fe, etc., were successfully coated on a variety of supports such as metal mesh and foams (e.g., Ni foam, Fe mesh, FeCrAl fiber, Al foils, etc.) with great potentials for different catalytic reactions [17–21]. Moreover, in-situ grown LDHs layers appeared to have strong adherence and mechanical stability between the layer and the metal substrate [22–24]. Notably, the formation of LDHs was influenced by different parameters such as reaction temperature, urea amount, metal concentration, and the ratio of trivalent and divalent ions [25,26]. However, researches on structured catalysts from in-situ grown precursors on the ceramic substrate via urea hydrolysis are rarely reported.

Recent innovative applications using structured catalysts and reactors for CO_2 methanation has been reviewed elsewhere [13]. Different catalytic systems were investigated, for example, the superior performance of honeycomb-type over powdered catalysts for the Sabatier reaction was confirmed at a very high gas space velocity (up to 50,000 h^{-1}) by Vita et al. [27] The authors studied Ni/Gd-CeO_2 catalysts on cordierite monolith prepared by solution combustion synthesis. Besides most honeycomb catalysts were prepared by washcoating the ready-made powdery catalysts onto monolithic surface using slurry solution. Janke et al. prepared cordierite honeycomb catalysts by slurry coating a commercial 10% Ru/γ-Al_2O_3 catalysts on the monolith [28]. Similar preparation was carried out by Fukuhara et al. that powder-type Ni-CeO_2 catalysts were slurry coated on aluminum honeycomb substrate [29,30]. Ahn et al. further studied the impact of different coating liquids when washcoating Ni-CeO_2 catalysts on the ceramic honeycomb monolith for CO_2 methanation [31]. To the best of our knowledge, monolithic catalysts derived from in-situ grown LDHs have not been employed for CO_2 methanation. Since the preparation of monolithic catalysts could significantly influence the catalytic performance [32,33], it would be important to study different synthesis methods.

In this work, we report a facile synthetic strategy of structured catalysts derived from in-situ grown NiFe LDHs precursors on washcoated cordierite monoliths. In general, the monolith was firstly washcoated using colloidal solutions, followed by urea hydrolysis in which a stable LDHs layer was formed. The influence of different colloidal coating, i.e., alumina or silica, on the synthesis of NiFe LDHs was studied. The impact of the metal concentration during urea hydrolysis was also investigated. After calcination and reduction, the well-dispersed NiFe active phases on cordierite monoliths were obtained and tested for CO_2 methanation under industrial relevant conditions.

2. Experimental

2.1. Materials

The cylindrical honeycomb monoliths were made of cordierite (Versagrid™, $MgO:SiO_2:Al_2O_3$ = 13.8:50:34 wt%,

and traces amount of iron and zinc oxide) supplied by Applied Ceramics Inc. (USA). The dimension of monoliths was 19 mm in diameter and 20 mm in length. The monoliths had 230 cells per square inch (cpsi), channel wall thickness of 200 ± 50 μm, average pore diameter of 4.5 μm, open frontal area of 72%, and geometric surface area of 2220 m^2 m^{-3}. All monoliths were washed with ethanol and water in an ultrasonic bath three times and dried at 90 °C overnight prior to further synthesis steps.

All reagents used for the synthesis of LDHs, i.e., urea, $Ni(NO_3)_2 \cdot 6H_2O$, $Fe(NO_3)_3 \cdot 9H_2O$ were analytical grade (Merck Millipore) and used as received without purification.

2.2. Coating on ceramic monoliths using colloidal solutions

In order to increase the surface area of the cordierite monolith, a washcoat layer of support material was deposited by dip coating method. Two different colloidal solutions were investigated, i.e., alumina and silica. Colloidal Al_2O_3 (Alfa Aesar, 20 wt% suspension in water, viscosity of 10 cps) has a particle size of 50 nm, while colloidal SiO_2 (LUDOX TM-50, 50 wt% suspension in water, viscosity of 55 cps) has a particle size of around 22–25 nm. In a typical dip coating cycle, the monolith was immersed in the colloidal solution for 3 min, then dried at 250 °C for 15 min. Several cycles were made to achieve the desired washcoat loading. Finally, the monolith was calcined at 600 °C for 6 h (heating rate of 2 K min^{-1}) in a muffle furnace. The washcoated monoliths are named COR-AluCC and COR-SiCC.

2.3. In-situ grown of LDHs layers on washcoated ceramic monoliths

Typically, aqueous stock solutions consisting of nickel nitrate, iron nitrate, and urea with a total molar concentration of 0.5 M or 0.05 M were used. The molar ratio of Ni^{2+}/Fe^{3+} was maintained at 4 and the molar ratio of urea and metal ion was 9.9, corresponding to a urea/nitrate ion ratio of 4.5. The selected urea/metal compositions had been optimized experimentally in order to obtain a pure LDHs structure.

The pretreated monolith was immersed in 45 mL of the stock solution, and subsequently transferred into a 90-mL Teflon-lined hydrothermal autoclave and heated at 110 °C for 24 h. After cooling the autoclave to room temperature, the monolith was washed with deionized water and dried at 90 °C for 1 h. Calcination was carried out at 600 °C for 6 h (heating rate of 2 K min^{-1}) in a muffle furnace. The final monolithic catalysts were designated as COR-AluCC-*x*M and COR-SiCC-*x*M, where *x* is the total metal concentration used in urea hydrolysis.

For comparison, the same synthesis procedure was conducted without the addition of washcoated monoliths. The solid precipitate was collected by centrifugation, washed, and dried. These LDHs powders are denominated as LDH-*x*M, where *x* is the total metal concentration used in urea hydrolysis. Also, the dry LDHs powders were calcined at 600 °C for 6 h.

2.4. Catalysts characterization

X-ray diffraction (XRD) diffractograms were recorded on a Bruker D8 Advance micro-diffractometer, equipped with CuKα radiation source. The scanning speed was 1° min^{-1} over the range from 5° to 70°. The average crystallite size *d* was calculated by the Scherrer equation [34].

Temperature programmed reduction (TPR) of the calcined catalyst powders was carried out on Micromeritics Autochem II ASAP 2020 instrument, equipped with a thermal conductivity detector (TCD). In order to obtain reliable data [35], approximately 35 mg of the samples was used, which was degassed at 200 °C for 30 min prior to measurement. The TPR profiles were recorded from 50 °C to 950 °C in flowing H_2 (10 vol% H_2/Ar) at a heating rate of 10 K min^{-1}.

Simultaneous thermogravimetric (TG) and differential scanning calorimetry (DSC) analysis were conducted using Netzsch STA449 Jupiter F3 instrument. A 10-mg sample was used and heated up to 800 °C at a heating rate of 10 K min^{-1} in He flow (20 mL min^{-1}).

The adherence of the coating layer was evaluated by measuring the weight loss after ultrasonic treatment. The monolith catalysts were immersed in ethanol and then transferred to the ultrasonic bath (45 kHz, 600 W) at room temperature for 30 min. The monolith catalysts were dried at 90 °C for 1 h and the total weight loss was calculated.

The specific surface area was measured from the N_2 adsorption–desorption isotherms at −196 °C using the Brunauer-Emmet-Teller (BET) equation [36]. The samples were degassed at 150 °C overnight before the analysis was carried out on the Micromeritics Tristar II 3020 instrument. The pore volume and pore size distribution were estimated using the Barrett–Joyner–Halenda (BJH) method [37].

The coating morphology of the structured catalysts was examined by scanning electron microscopy (SEM, ZEISS Gemini Supra 35VP) equipped with energy dispersive X-ray spectrometry (EDX) for elemental mapping. Prior to analysis, the monolith was polished and coated with Pd plasma to inhibit charging.

2.5. Activity tests on the structured reactor

The structured reactor was made from stainless steel with an inner diameter of 21.1 mm and an outer diameter of 25.4 mm. The reactor was horizontally installed and heated by an electric oven, where the temperature was controlled by a thermocouple (type K) inside the reactor. The schematic representing the reactor setup is shown in Fig. 1a. Since the outer diameter of the monolith was 20 mm, an in-house designed catalyst holder with an inner diameter of 19.1 mm was used. Therefore, the structured catalysts were inserted in the holder and could be easily placed inside and removed from the reactor, avoiding any potential for gas channeling. Fig. 1b

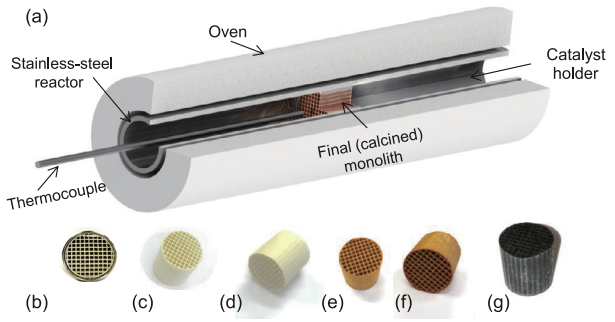

Fig. 1. (a) Schematic diagram of structured reactor setup; (b) photograph of monolith located inside the holder; (c-d) photograph of fresh cordierite monolith; (e-f) photograph of calcined monolith before reaction; (g) photograph of monolith after reaction.

illustrates the monolith inside the holder while photographs of fresh, calcined and spent monoliths are shown in Fig. 1c–f.

Prior to the reaction, the monolithic catalyst was reduced at 600 °C for 2 h in 50 vol% H_2/N_2 with a total flow of 200 mL min^{-1} (STP). Thereafter, the reactor was cooled down in pure N_2 flow for 2 h. Subsequently, a total flow of reactant gases of 500 mL min^{-1} (STP) was introduced, corresponding to a gas hourly space velocity (GHSV) of 7,760 h^{-1}. The ratio of $H_2/N_2/CO_2$ was 64/20/16 (i.e., $H_2/CO_2 = 4/1$). The reaction was carried out at 200–500 °C at ambient pressure and kept at each temperature for 1 h. Water formed during the reaction was removed by a cold trap. The outgas was analyzed using an online gas chromatograph (Agilent 7890A). A blank test was conducted, and no conversion was found over pure cordierite monolith in the stainless-steel reactor.

The CO_2 conversion (X_{CO_2}), CH_4 selectivity (S_{CH_4}), and CH_4 yield (Y_{CH_4}) were defined in Eqs. (2)–(4), where F^{in} and F^{out} are the molar flow rates in and out of the reactor (mol/h).

$$X_{CO_2}(\%) = \frac{F^{in}_{CO_2} - F^{out}_{CO_2}}{F^{in}_{CO_2}} \times 100 \quad (2)$$

$$S_{CH_4}(\%) = \frac{F^{out}_{CH_4}}{F^{in}_{CO_2} - F^{out}_{CO_2}} \times 100 \quad (3)$$

$$Y_{CH_4}(\%) = \frac{F^{out}_{CH_4}}{F^{in}_{CO_2}} \times 100 \quad (4)$$

3. Results and discussion

3.1. Characterization of NiFe LDHs

The XRD diffractograms of the dry powder obtained after urea hydrolysis were shown in Fig. 2. The characteristic peaks of LDHs structures were observed for both LDH-0.5M and LDH-0.05M samples with symmetric and sharp reflections of the basal (003), (006), (012) planes at 2θ of 11.3°, 22.9°, and 34.4°, respectively (MgAl-CO_3 LDHs, JCPDS 01-089-0460). Other peaks were ascribed to the nonbasal (015), (018), (110), and (113) planes. No other impure phases such as $Ni(HCO_3)_2$

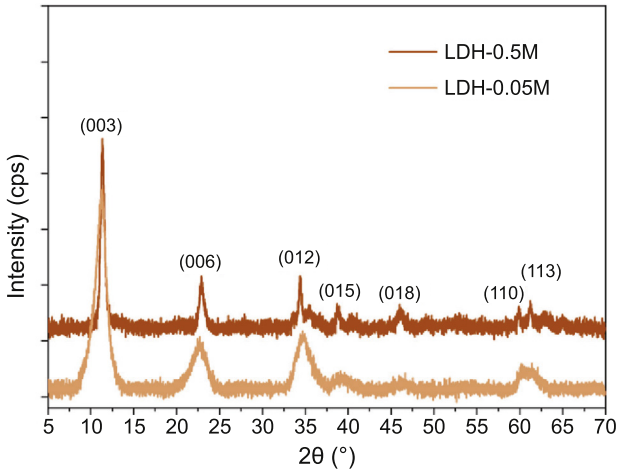

Fig. 2. XRD diffractograms of NiFe LDHs prepared by urea hydrolysis.

were detected [38]. Therefore, it can be confirmed that NiFe LDHs with high purity and crystallinity were successfully synthesized via urea hydrolysis at both total metal concentration of 0.5 M and 0.05 M.

The crystallite size in the stacking direction of LDH-0.5M was 16 nm, calculated by the Scherrer equation on the (003) diffraction. By diluting the stock solution, the LDHs particle size reduced significantly to only 6 nm. Moreover, it is worth mentioning that the pH of the stock solution was initially around 2.4–2.7. After 24 h of decomposition at 110 °C, the pH of the solution underwent a steep increase to 8.8–8.5, confirming the precipitation of both Ni^{2+} and Fe^{3+} ions [38].

The thermal decomposition of NiFe LDHs was analyzed by TG and DSC (Fig. 3). The TG curves of both LDHs sample shows common features for the decomposition of the layered structure [39]. Initially, physisorbed water and water in the interlayer were removed at 150–250 °C. Subsequently, dehydroxylation and decarbonation occurred simultaneously up to 500 °C. The total weight loss of LDH-0.05M was higher than LDH-0.5M, which could be ascribed to a higher amount of

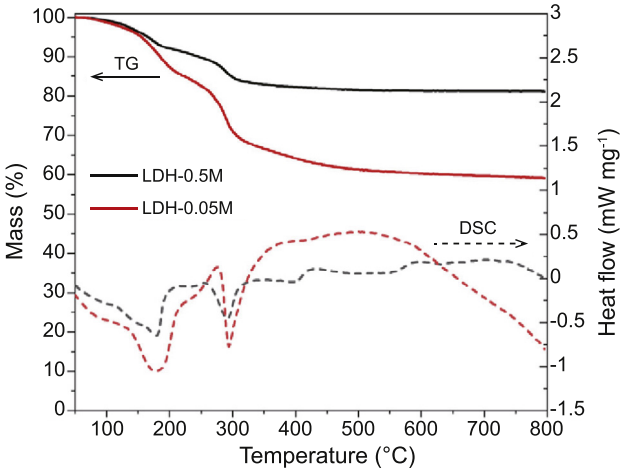

Fig. 3. Thermal analysis (TG and DSC) of NiFe LDHs.

water, hydroxyl, and anion in the interlayer [40,41]. In addition, the DSC curves display two endothermic peaks for both samples, corresponding to the two stages of weight loss. The high intensity of the peaks was also related to the high crystallinity of the samples, which is consistent with the XRD analysis (Fig. 2).

From the TG analysis, calcination at 600 °C would be sufficient for the decomposition of LDHs. Moreover, XRD analysis of calcined LDHs confirmed that LDHs structures were completely transformed into mixed metal oxides since only diffraction patterns of $NiFe_2O_4$ (JCPDS 00-054-0964) and NiO (JCPDS 01-089-5881) were identified (Fig. 4). The crystallite size of calcined LDH-0.5M was 22 nm, estimated by the Scherrer equation at 2θ of 43.4°. On the other hand, the crystallite size of LDH-0.05M was only 11 nm. Overall, increasing the concentration of stock solution would enlarge the particle size of LDHs [26].

To study the reducibility of the mixed oxides derived from LDHs, H_2-TPR analysis was performed (Fig. 5). Pure NiO was reported to be reduced at 340–410 °C, while Fe_2O_3 had a sequential reduction at 380 °C, 620 °C, and 715 °C [12,42]. However, the reduction of Fe was strongly enhanced in the presence of Ni that a gradual shift to lower temperature of reduction peaks would be observed [43]. As the theoretical weight percentage of Ni was 79 wt.%, the TPR profiles would show a similar pattern to the reduction of Ni species [44]. The first peak and the last peak in Fig. 5 could be assigned to the reduction of Fe^{3+} to $Fe^{8/3+}$ and Fe^{2+} to Fe, respectively. Two peaks at 350–450 °C were ascribed to the reduction of $Fe^{8/3+}$ and Ni^{2+} species in $NiFe_2O_4$ and NiO [45]. The peaks of LDH-0.05M were located at lower temperatures than that of LDH-0.5M, implying that the former was easier to be reduced than the latter.

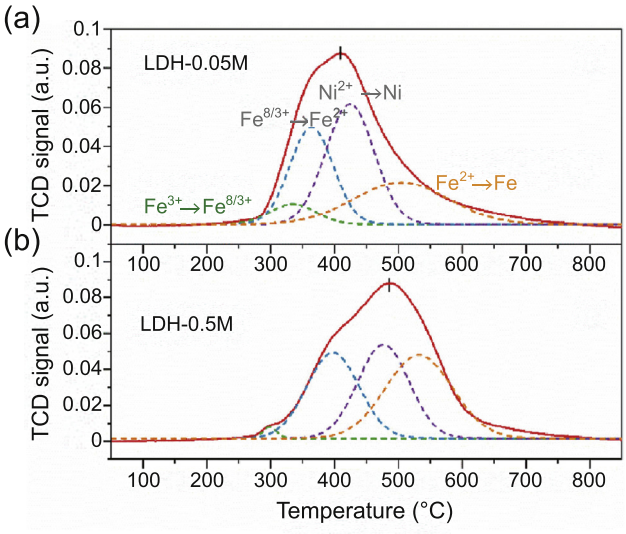

Fig. 5. TPR profiles of calcined (a) LDH-0.05M, and (b) LDH-0.5M.

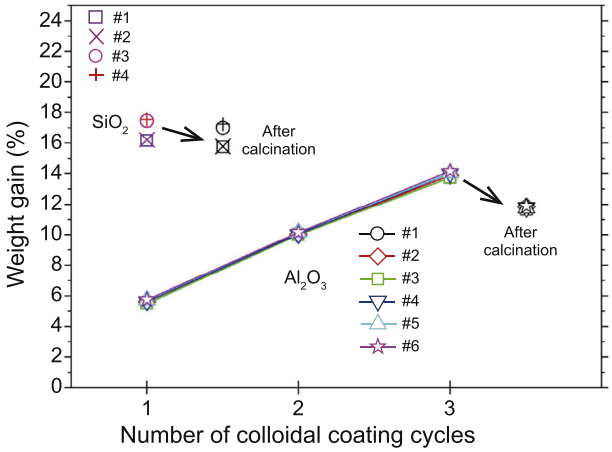

Fig. 6. The weight gain of monoliths after colloidal coating and calcination.

3.2. Characterization of the structured catalysts

3.2.1. Synthesis of the structured catalysts

The first step of structured catalysts preparation was dip coating support materials onto cordierite monoliths using colloidal solutions. The weight gain of monoliths after several colloidal coating cycles are presented in Fig. 6. For alumina coating, the washcoat layer reached 14 ± 0.5 wt% after three times of dip coating and drying. The weight gain of six

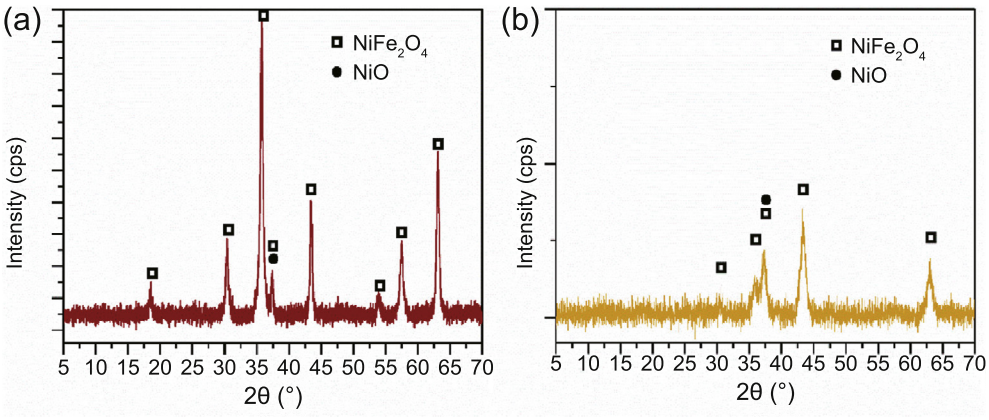

Fig. 4. XRD diffractograms of calcined NiFe LDHs: (a) LDH-0.5M and (b) LDH-0.05M.

different monoliths as shown in Fig. 6 demonstrates the high reproducibility of the synthesis procedure. On the other hand, one coating cycle was sufficient to achieve a washcoat layer of 17 ± 1 wt% for SiO_2, where the reproducibility was also confirmed by four monolith samples. Calcination was subsequently conducted for the fixation of the support materials onto cordierite. As a result, the weight of washcoat layers was reduced to 12 wt% for COR-AluCC and 16 wt% for COR-SiCC.

In the second step, NiFe LDHs were in-situ grown on the washcoated monoliths by urea hydrolysis at 110 °C for 24 h. After washing, drying, and calcination, the mixed oxides layer was fixed on the cordierite monoliths. The catalyst loading was defined as the percentage of the catalytic mass (mixed oxides) on the total weight of the final monolith, and the results are summarized in Table 1. It can be seen that Al_2O_3 was more advantageous for the deposition of the catalyst layer than SiO_2, even though SiO_2 was easier to be washcoated on the monolith.

3.2.2. Mechanical stability of the catalytic layers on the monoliths

In industrial applications, monolithic catalysts may experience different severe stresses such as thermal, chemical, and mechanical stresses. For gas-phase processes like methanation unit in PtG technology under stationary operating conditions, thermal and chemical stresses could be ruled out. However, mechanical stress can affect the amount of active phase on the washcoated monoliths. Ultrasonic vibration test is often used to estimate the effect of mechanical stress on the monoliths [46]. The adherence of the catalytic layer, calculated by the weight loss percentage, is reported in Table 1 for the calcined structured catalysts.

The adherence of the NiFe oxides layer on alumina-washcoated cordierite substrate was relatively high at 99.2% for COR-AluCC-0.5M and 99.6% for COR-AluCC-0.05M. By using stock solutions of 0.05 M, less amount of LDHs was deposited, which could be the reason for the stronger anchoring forces on the substrate. On the other hand, the COR-SiCC-0.5M showed slightly weaker adhesion. Nevertheless, the catalyst layer prepared by hydrothermal synthesis on the ceramic monoliths had good mechanical stability, similar to those prepared on metallic monoliths [22,23].

3.2.3. Textural properties of the structured catalysts

It is well-known that cordierite monoliths have an ultralow BET surface area, which was 1.2 $m^2\ g^{-1}$ in this study. After washcoating alumina and silica on the substrate, the surface area of COR-AluCC and COR-SiCC was larger at 18.3 $m^2\ g^{-1}$ and 17.0 $m^2\ g^{-1}$, respectively (Table 2). Thereafter, when LDH-0.5M was grown on the monolith and calcined, the surface area of both COR-AluCC and COR-SiCC further increased to 30.7 $m^2\ g^{-1}$ and 34.8 $m^2\ g^{-1}$, respectively. The pore volume of the final monolithic catalysts was larger than that of washcoated monoliths. For COR-AluCC-0.05M, the structured catalyst had a similar surface area yet slightly smaller pore volume than COR-AluCC.

Table 2
Textural properties of the washcoated monoliths and final calcined structured catalysts.

Samples	BET specific surface area ($m^2\ g^{-1}_{\text{total COR}}$)	BJH pore volume ($cm^3\ g^{-1}$)
COR-AluCC	18.3	0.064
COR-SiCC	17.0	0.045
COR-AluCC-0.5M	30.7	0.069
COR-AluCC-0.05M	18.3	0.047
COR-SiCC-0.5M	34.8	0.070

Cordierite monolith had a very low macropore volume with an average macropore size of 4.5 μm. In this study, the micro-mesopore size of washcoated and final monoliths was calculated from the N_2 physisorption isotherms using the BJH method. The COR-AluCC washcoated monoliths had an average pore size of 9 nm, while it was smaller at 7 nm for COR-SiCC (Fig. 7). After LDHs layers were formed and calcined, the pore sizes were reduced for both COR-AluCC-0.5M and COR-AluCC-0.05M, and obviously less for the latter. A bimodal pore size distribution of 4 nm and 6 nm was observed for COR-SiCC-0.5M and the pore sizes were also reduced compared to COR-SiCC.

3.2.4. Morphology of the structured catalysts

The in-situ grown LDHs structure was examined by SEM characterization (Fig. 8). For COR-AluCC-0.5M, the monolithic surface contained numerous hexagonal platelets intercrossed with each other, which was typical morphology of LDHs prepared by urea hydrolysis [47]. The lateral size of these platelets was around 1 μm (900 ± 100 nm), while the thickness was 30 ± 10 nm. When LDHs were formed using a diluted stock solution, the hexagonal platelets were smaller with a lateral diameter at 300 ± 50 nm, while the thickness was maintained at 35 ± 10 nm (COR-AluCC-0.05M, Fig. 8b). This is also consistent with the observed trend based on XRD study (Fig. 2). Hence, smaller LDHs particles were obtained at a lower metal concentration [24,26,48]. For COR-SiCC-0.5M

Table 1
Synthesis parameters, mass of in-situ grown LDHs, catalyst loading and the adherence of structured catalysts.

Structured catalysts	Colloidal solution	Total metal concentration	Mass of LDHs (mg)	Catalyst loading (wt%)	Adherence % (Weight loss %)
COR-AluCC-0.5M	Al_2O_3	0.5 M	175.8	2.85%	99.2% (0.8%)
COR-AluCC-0.05M	Al_2O_3	0.05 M	60.1	0.58%	99.6% (0.4%)
COR-SiCC-0.5M	SiO_2	0.5 M	112.8	2.24%	98.9% (1.1%)

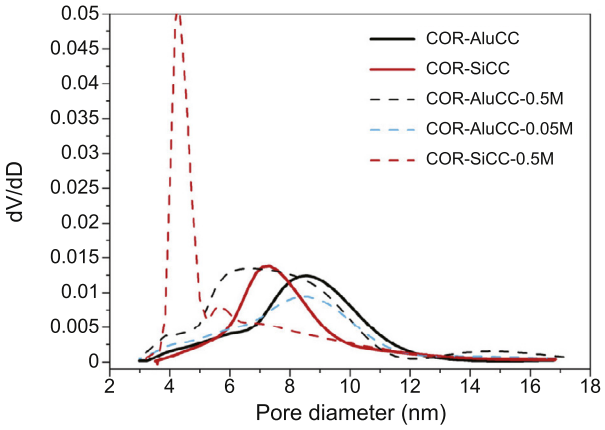

Fig. 7. Pore size distribution of washcoated monoliths and final structured catalysts.

(Fig. 8c), the regular flower-like clusters of NiFe LDHs were 2–3 times smaller as compared to COR-AluCC-0.5M. The thickness of the platelets was about 20–30 nm while the lateral dimension was difficult to measure.

The morphology of the final monolithic catalyst was also of great interest. Fig. 8d reveals that although significantly reduced in lateral size, the mixed oxides particles were still in its original hexagonal shape after calcination. This is beneficial for the dispersion of Ni and Fe active sites. Moreover, the ordered interconnection between the platelets was maintained, providing sufficient exposed surface area for reactant molecules to access to the active sites.

Furthermore, the cross-sectional SEM images of the channel wall were captured, and EDX elemental mapping was conducted. It is noteworthy that the washcoat layer using colloidal solutions of alumina and silica could not be observed or differentiated from cordierite ($2MgO \cdot 5SiO_2 \cdot 2Al_2O_3$). For COR-AluCC-0.5M, the deposition–precipitation of LDHs occurred on the porous exterior. Fig. 9a combined with Fig. 8a suggests that the LDHs platelets were grown perpendicularly on the cordierite surface, which could be explained by the evolution selection mechanism [22].

The LDHs layer on COR-AluCC-0.5M was around 20 μm, which was relatively thin compared to the channel wall thickness of 200 ± 50 μm. Moreover, the EDX mapping images show a spatial distribution of Ni and Fe on the LDHs region without visible segregation, demonstrating well-dispersed metal ions of LDHs.

For COR-SiCC-0.5M, the thickness of LDHs layers located outside the cordierite wall was similar at 15–27 μm. However, the elemental mapping detected both Ni and Fe even inside the pores of cordierite, which was not the case for COR-AluCC-0.5M. Thus, it could be assumed that Ni and Fe were diffused into the porous structure and LDHs layer deposited both inside the pore and on the surface of the monolith. This further explains why smaller pores were obtained for COR-SiCC-0.5M from the pore size distribution analysis (Fig. 7).

LDHs could only deposit due to chemical bonding between the material itself and the substrate surface, especially on a polar substrate [49]. Reports showed that LDHs were not feasible to grow on an un-anodized aluminum substrate [23], or FeCrAl-fiber without Al_2O_3 washcoat [20]. In this work,

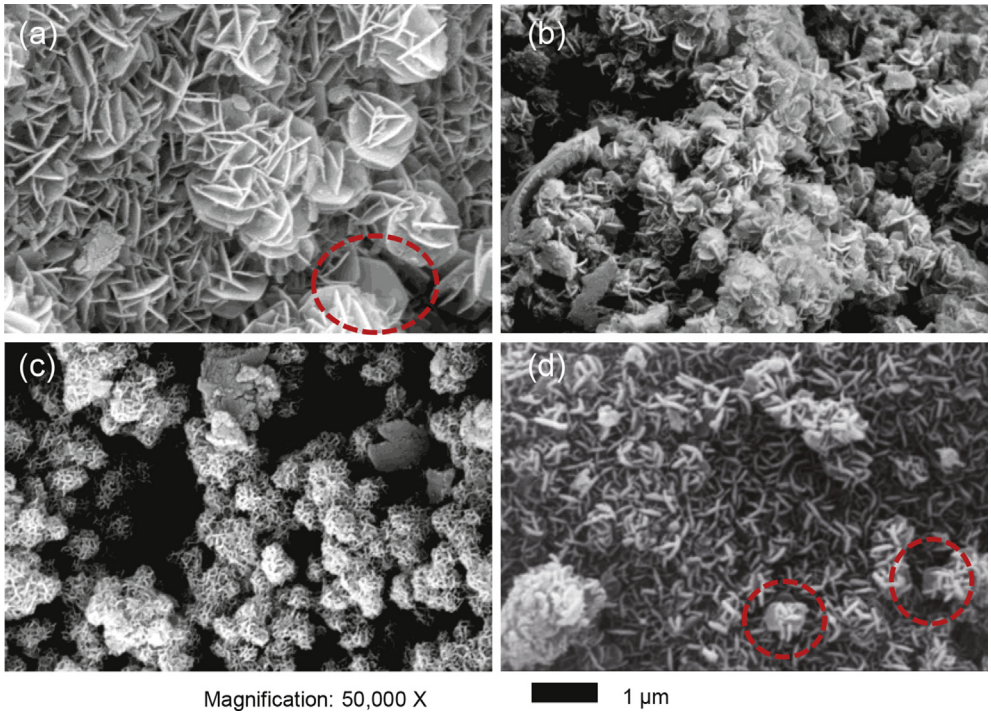

Fig. 8. SEM images of in-situ grown LDHs on monoliths of (a) COR-AluCC-0.5M, (b) COR-AluCC-0.05M, (c) COR-SiCC-0.5M and (d) calcined COR-AluCC-0.5M.

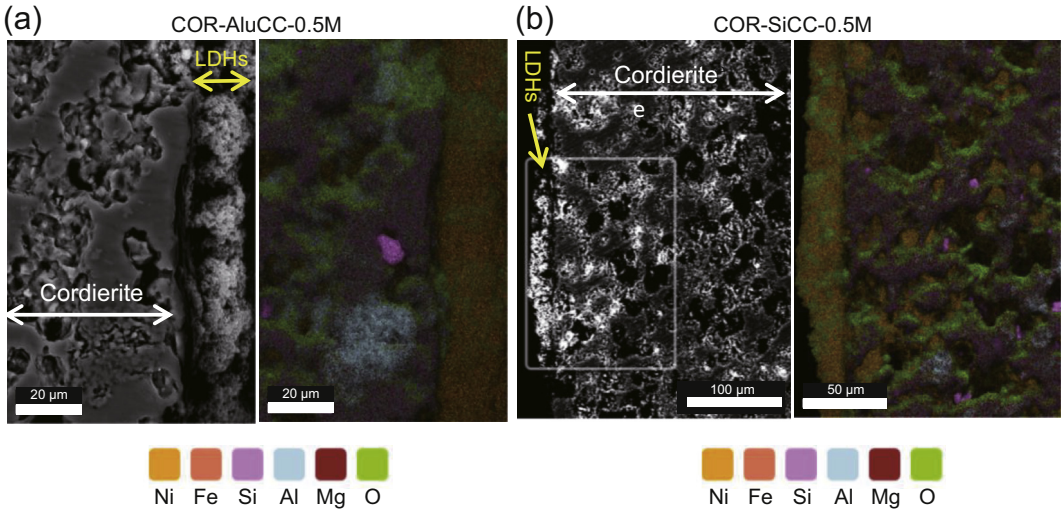

Fig. 9. SEM images and corresponding EDX elemental mapping of the cross-sectional channel wall of (a) COR-AluCC-0.5M and (b) COR-SiCC-0.5M monolith.

colloidal solutions with conductive properties should have played an important role in the anchoring of NiFe LDHs on the ceramic monoliths. In fact, SiO_2 nanoparticles (~25 nm, high viscosity) had a negative charge while Al_2O_3 nanoparticles (~50 nm, low viscosity) had a positive charge. The higher viscosity of silica colloidal could explain the successful ~17 wt% loading after one washcoating cycle, compared to three cycles of COR-AluCC [50]. Smaller silica particles could have diffused further inside the pore of cordierite monolith.

For COR-AluCC-0.05M, since a very diluted stock solution was used during urea hydrolysis, the in-situ grown LDHs layer at very low weight loading was unable to be observed from SEM imaging (Fig. 10). Although the thickness was not measurable, LDHs were found to be distributed on the surface of the porous cordierite, similar to COR-AluCC-0.5M.

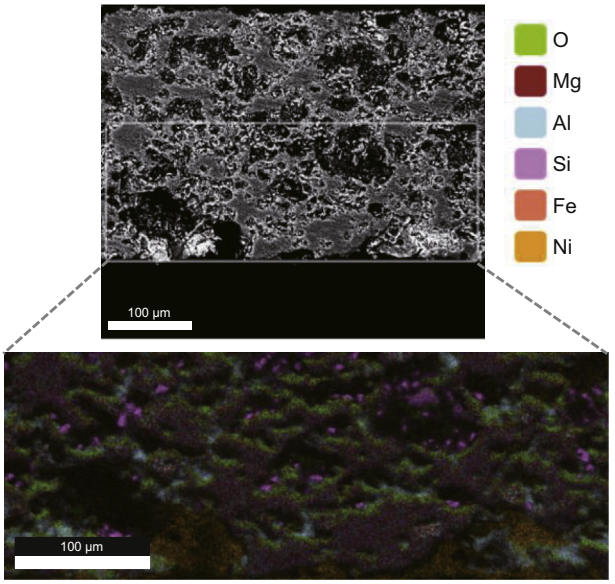

Fig. 10. SEM images and corresponding EDX elemental mapping of the cross-sectional channel wall of COR-AluCC-0.05M monolith.

3.3. Catalytic performance of the structured catalysts

The reaction was carried out at a temperature range of 200–500 °C with a total gas flow of 500 mL min^{-1} (STP). Although the monoliths had different coating thickness, the final monolithic catalysts were considered to have the same bulk volume. Accordingly, GHSV was calculated to be 7,760 h^{-1}. The active phase on the monoliths was assumed to be stable during the reaction at this high GHSV due to insignificant weight loss, as summarized in Table 3. Furthermore, the weight losses were mainly due to the reduction of oxides into metallic phases.

CO_2 conversion, CH_4 selectivity and CH_4 yield from CO_2 methanation over the monolithic catalysts are shown in Figs. 11, 12 and 13, respectively. Although CO_2 methanation was thermodynamically favored at low temperatures, it was difficult to achieve high CO_2 conversion due to kinetic barriers. As expected, all monolithic catalysts exhibited low activity at 200–250 °C. Interestingly, at 300 °C, COR-AluCC-0.5M showed excellent activity with the highest CO_2 conversion of 70%, while the other two showed poorer performance (Fig. 11). Although COR-SiCC-0.5M had much higher catalyst loading than COR-AluCC-0.05M, the former exhibited lower CO_2 conversion, especially at 350–450 °C. At higher temperature of 400–500 °C, the conversion started to decrease following the thermodynamic equilibrium curve.

During CO_2 hydrogenation to CH_4, reverse water gas shift reaction ($CO_2 + H_2 \leftrightarrow CO + H_2O$) could simultaneously

Table 3
Weight loss of structured catalysts after temperature-programmed CO_2 methanation at GHSV of 7,760 h^{-1}, atmospheric pressure.

Structured catalysts	Weight loss (%)[a]
COR-AluCC-0.5M	0.7
COR-AluCC-0.05M	0.4
COR-SiCC-0.5M	0.5

[a] weight loss = (weight $_{\text{total COR before}}$ − weight $_{\text{total COR after}}$)/ weight $_{\text{total COR before}}$.

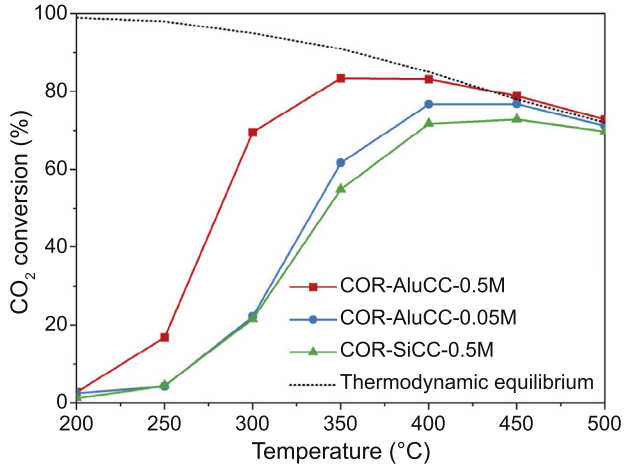

Fig. 11. CO_2 conversion of structured catalysts in CO_2 methanation at atmospheric pressure, GHSV of 7,760 h^{-1}, $H_2/N_2/CO_2$ = 64/20/16 vol%. The thermodynamic equilibrium conversion curve is also included for comparison.

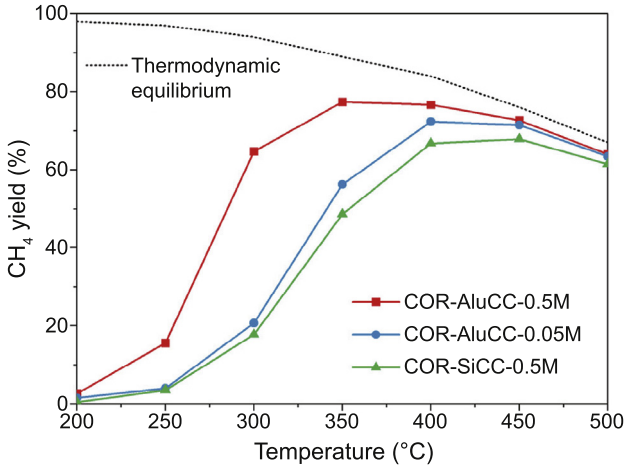

Fig. 13. CH_4 yield of structured catalysts in CO_2 methanation at atmospheric pressure, GHSV of 7,760 h^{-1}, $H_2/N_2/CO_2$ = 64/20/16 vol%. The thermodynamic equilibrium of CH_4 yield is also included for comparison.

occur which suppressed the formation of CH_4. Thus, CH_4 selectivity was an important indicator when evaluating structured catalysts for CO_2 methanation. The catalysts on COR-AluCC monoliths showed good selectivity towards methane (>90%) at 250–500 °C, demonstrating that CO_2 methanation was dominant under the reaction condition (Fig. 12). On the other hand, at 250–400 °C, lower CH_4 selectivity was obtained over COR-SiCC-0.5M.

The best catalytic performance of COR-AluCC-0.5M amongst others was confirmed by the methane yield (Fig. 13). This could be explained by the fact that COR-AluCC-0.5M had the highest catalyst loading with a thin and well-adhered layer on the honeycomb substrate. As for COR-AluCC-0.05M, the low-loading monolith exhibited even higher methane yield than that of COR-SiCC-0.5M.

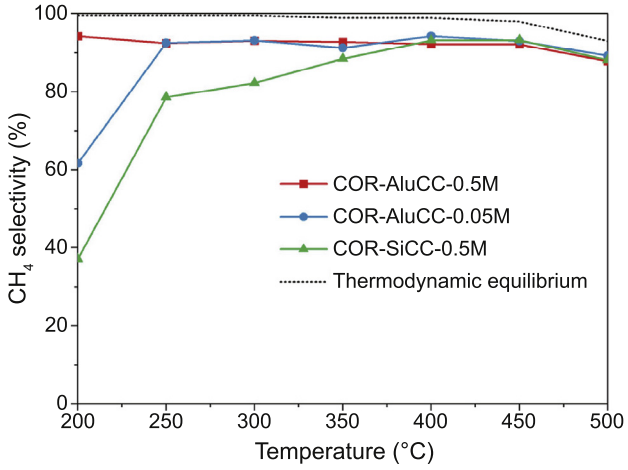

Fig. 12. CH_4 selectivity of structured catalysts in CO_2 methanation at atmospheric pressure, GHSV of 7,760 h^{-1}, $H_2/N_2/CO_2$ = 64/20/16 vol%. The thermodynamic equilibrium of CH_4 selectivity is also included for comparison.

Interestingly, COR-SiCC-0.5M contained similar content of the active phase as COR-AluCC-0.5M but its catalytic performance was much poorer. The EDX elemental mapping (Fig. 9b) revealed a large amount of Ni and Fe penetrated inside the pore structure of cordierite. These active sites would be more difficult to be reached by gaseous molecules. As a result, the diffusion path could be extended from the exterior (20 μm) to the whole channel wall thickness (200 ± 50 μm). Therefore, COR-SiCC-0.5M had lower methane yield even compared to COR-AluCC-0.05M. It is noteworthy that the higher activity of COR-AluCC-0.5M could also be due to the stronger metal-support interaction of Al_2O_3 than SiO_2 in supported catalysts [51,52].

It is important to note that a high reproducibility was achieved in terms of preparation and activity test of structured catalysts. The reproduced experimental data are reported in Table S1 and Fig. S1 in the supporting information.

4. Conclusions

A facile preparation method of structured catalysts for CO_2 methanation was developed. The thin layer of NiFe LDHs was successfully in-situ grown with excellent adherence to the washcoated cordierite monoliths via urea hydrolysis. Under CO_2 methanation reaction at high gas velocity, the catalytic layer exhibited higher activity on Al_2O_3-washcoated than SiO_2-washcoated monolith. It could be due to Al_2O_3 was only washcoated on the exterior of the monolith and the diffusion path for reactant gases was much shorter during methanation. A suitable high-concentration stock solution is also advantageous to achieve high catalyst loading on the ceramic monolith, thus high methane yield in CO_2 methanation. Therefore, COR-AluCC-0.5M monolithic catalyst is promising for the development of industrial high-throughput methanation reactor, an important unit of the PtG technology. The synthetic

strategy developed in this work could also be utilized to prepare structured catalysts for other catalytic processes.

Conflict of interest

The authors declare no conflict of interests.

Acknowledgments

The authors would like to thank the Norwegian Ministry of Education and Research for financial support.

Appendix A. Supplementary data

Supplementary data to this article can be found online at https://doi.org/10.1016/j.gee.2020.09.004.

References

[1] D. Reichle, J. Houghton, B. Kane, J. Ekmann, Carbon sequestration research and development, Oak Ridge National Lab., TN (US), 1999.
[2] S. Rönsch, J. Schneider, S. Matthischke, M. Schlüter, M. Götz, J. Lefebvre, P. Prabhakaran, S. Bajohr, Fuel 166 (2016) 276–296.
[3] P. Sabatier, J.B. Senderens, Comptes Rendus Acad. Sci. 1902, Section VI - Chimie 514–517.
[4] C. Vogt, M. Monai, G.J. Kramer, B.M. Weckhuysen, Nat. Catal. 2 (2019) 188–197.
[5] M.a.A. Aziz, A.A. Jalil, S. Triwahyono, A. Ahmad, Green Chem. 17 (2015) 2647–2663.
[6] M. Bailera, P. Lisbona, L.M. Romeo, S. Espatolero, Renew. Sustain. Energy Rev. 69 (2017) 292–312.
[7] K. Ghaib, F.Z. Ben-Fares, Renew. Sustain. Energy Rev. 81 (2018) 433–446.
[8] P. Frontera, A. Macario, M. Ferraro, P. Antonucci, Catalysts 7 (2017) 59.
[9] C. Lv, L. Xu, M. Chen, Y. Cui, X. Wen, Y. Li, C.E. Wu, B. Yang, Z. Miao, X. Hu, Q. Shou, Front. Chem. (2020). https://www.frontiersin.org/articles/10.3389/fchem.2020.00269/full.
[10] M.P. Andersson, T. Bligaard, A. Kustov, K.E. Larsen, J. Greeley, T. Johannessen, C.H. Christensen, J.K. Nørskov, J. Catal. 239 (2006) 501–506.
[11] A.L. Kustov, A.M. Frey, K.E. Larsen, T. Johannessen, J.K. Nørskov, C.H. Christensen, Appl. Catal. Gen. 320 (2007) 98–104.
[12] D. Pandey, K. Ray, R. Bhardwaj, S. Bojja, K.V.R. Chary, G. Deo, Int. J. Hydrogen Energy 43 (2018) 4987–5000.
[13] H.L. Huynh, Z. Yu, Energy Technol. 8 (2020) 1901475.
[14] M. Lehner, R. Tichler, H. Steinmüller, M. Kopper (Eds.), in: The Power-to-Gas Concept, SpringerBriefs in Energy. Springer, Cham. 2014, pp. 41–61.
[15] E. Tronconi, G. Groppi, C.G. Visconti, Curr. Opin. Chem. Eng. 5 (2014) 55–67.
[16] T.A. Nijhuis, A.E.W. Beers, T. Vergunst, I. Hoek, F. Kapteijn, J.A. Moulijn, Catal. Rev. 43 (2001) 345–380.
[17] H. Chen, L. Hu, M. Chen, Y. Yan, L. Wu, Adv. Funct. Mater. 24 (2014) 934–942.
[18] W. Li, G. Fan, L. Yang, F. Li, ChemCatChem 8 (2016) 2724–2733.
[19] H. Li, D. Zhang, P. Maitarad, L. Shi, R. Gao, J. Zhang, W. Cao, Chem. Commun. 48 (2012) 10645–10647.
[20] R. Chai, S. Fan, Z. Zhang, P. Chen, G. Zhao, Y. Liu, Y. Lu, ACS Sustain. Chem. Eng. 5 (2017) 4517–4522.
[21] H. Chen, F. Zhang, S. Fu, X. Duan, Adv. Mater. 18 (2006) 3089–3093.
[22] X. Guo, S. Xu, L. Zhao, W. Lu, F. Zhang, D.G. Evans, X. Duan, Langmuir 25 (2009) 9894–9897.
[23] Z. Lü, F. Zhang, X. Lei, L. Yang, S. Xu, X. Duan, Chem. Eng. Sci. 63 (2008) 4055–4062.
[24] T. Xue, R. Li, Y. Gao, Q. Wang, Chem. Eng. J. 384 (2020) 123284.
[25] M. Adachi-Pagano, C. Forano, J.-P. Besse, J. Mater. Chem. 13 (2003) 1988–1993.
[26] M. Ogawa, H. Kaiho, Langmuir 18 (2002) 4240–4242.
[27] A. Vita, C. Italiano, L. Pino, P. Frontera, M. Ferraro, V. Antonucci, Appl. Catal. B Environ. 226 (2018) 384–395.
[28] C. Janke, M.S. Duyar, M. Hoskins, R. Farrauto, Appl. Catal. B Environ. 152–153 (2014) 184–191.
[29] C. Fukuhara, K. Hayakawa, Y. Suzuki, W. Kawasaki, R. Watanabe, Appl. Catal. Gen. 532 (2017) 12–18.
[30] S. Ratchahat, M. Sudoh, Y. Suzuki, W. Kawasaki, R. Watanabe, C. Fukuhara, J. CO_2 Util. 24 (2018) 210–219.
[31] J.Y. Ahn, S.W. Chang, S.M. Lee, S.S. Kim, W.J. Chung, J.C. Lee, Y.J. Cho, K.S. Shin, D.H. Moon, D.D. Nguyen, Fuel 250 (2019) 277–284.
[32] V. Meille, Appl. Catal. Gen. 315 (2006) 1–17.
[33] P. Avila, M. Montes, E.E. Miró, Chem. Eng. J. 109 (2005) 11–36.
[34] U. Holzwarth, N. Gibson, Nat. Nanotechnol. 6 (2011) 534-534.
[35] A. Gervasini, A. Auroux, Ed. UK (2013).
[36] S. Brunauer, P.H. Emmett, E. Teller, J. Am. Chem. Soc. 60 (1938) 309–319.
[37] E.P. Barrett, L.G. Joyner, P.P. Halenda, J. Am. Chem. Soc. 73 (1951) 373–380.
[38] X. Wu, Y. Du, X. An, X. Xie, Catal. Commun. 50 (2014) 44–48.
[39] F. Cavani, F. Trifirò, A. Vaccari, Catal. Today 11 (1991) 173–301.
[40] H. Wang, G. Fan, C. Zheng, X. Xiang, F. Li, Ind. Eng. Chem. Res. 49 (2010) 2759–2767.
[41] H. Wang, J. Gao, Z. Li, Y. Ge, K. Kan, K. Shi, CrystEngComm 14 (2012) 6843–6852.
[42] D. Beierlein, D. Häussermann, M. Pfeifer, T. Schwarz, K. Stöwe, Y. Traa, E. Klemm, Appl. Catal. B Environ. 247 (2019) 200–219.
[43] D. Shi, R. Wojcieszak, S. Paul, E. Marceau, Catalysts 9 (2019) 451.
[44] R. Brown, M.E. Cooper, D.A. Whan, Appl. Catal. 3 (1982) 177–186.
[45] T. Li, H. Wang, Y. Yang, H. Xiang, Y. Li, Fuel Process. Technol. 118 (2014) 117–124.
[46] D. Wu, Y. Zhang, Y. Li, J. Ind. Eng. Chem. 56 (2017) 175–184.
[47] Y. Han, H. Li, X. Ma, Z.H. Liu, Solid State Sci. 11 (2009) 2149–2155.
[48] J. Liu, Y. Li, X. Huang, G. Li, Z. Li, Adv. Funct. Mater. 18 (2008) 1448–1458.
[49] J.A. Gursky, S.D. Blough, C. Luna, C. Gomez, A.N. Luevano, E.A. Gardner, J. Am. Chem. Soc. 128 (2006) 8376–8377.
[50] C. Agrafiotis, A. Tsetsekou, I. Leon, J. Am. Ceram. Soc. 83 (2000) 1033–1038.
[51] D. Pandey, G. Deo, Chem. Eng. Commun. 203 (2016) 372–380.
[52] I. Wysocka, J. Hupka, A. Rogala, Catalysts 9 (2019) 540.